

Advanced Visibility Improvement Based on Polarization Filtered Images

Einav Namer and Yoav Y. Schechner

Dept. Electrical. Eng., Technion - Israel Institute of Technology, Haifa, ISRAEL

ABSTRACT

Recent studies have shown that major visibility degradation effects caused by haze can be corrected for by analyzing polarization-filtered images. The analysis is based on the fact that the path-radiance in the atmosphere (airlight) is often partially polarized. Thus, associating polarization with path-radiance enables its removal, as well as compensation for atmospheric attenuation. However, prior implementations of this method suffered from several problems. First, they were based on mechanical polarizers, which are slow and rely on moving part. Second, the method had failed in image areas corresponding to specular objects, such as water bodies (lakes) and shiny construction materials (e.g., windows). The reason for this stems from the fact that specular objects reflect partially polarized light, confusing a naive association of polarization solely with path-radiance. Finally, prior implementations derived necessary polarization parameters by manually selecting reference points in the field of view. This human intervention is a drawback, since we would rather automate the process. In this paper, we report our most recent progress in the development of our visibility-improvement method. We show directions by which those problems can be overcome. Specifically, we added algorithmic steps which automatically extract the polarization parameters needed, and make visibility recovery more robust to polarization effects originating from specular objects. In addition, we now test an electrically-switchable polarizer based on a liquid crystal device for improving acquisition speed.

Keywords: Computer vision, Polarization-imaging, Image processing, Atmospheric haze, Image recovery, Scattering, Turbid media, Color.

1. INTRODUCTION

There is a growing interest in the automatic analysis of images acquired in scattering media.^{4, 8, 12, 14} A main objective in such analysis is improvement of visibility and recovery of colors, as if imaging is done in clear conditions. Computer vision and human vision can then capitalize on such improved images for various applications, such as long range surveillance, targets detection and recognition, navigation and photography.

To achieve this goal, some methods are based on specialized radiation hardware. Others are based on pure mathematical processing of images.⁷ In contrast, Ref. 13 proposed a method that is based on simple acquisition hardware, coupled to a mathematical algorithm. It is a passive computer vision approach, exploiting polarization effects in natural illumination. In addition to image recovery, this method recovers a distance map of the scene.

The method in Ref. 13 has demonstrated very effective results. However, it relies on several simple assumptions that are sometimes violated. For example, one assumption is that polarization in the scene is associated with ambient illumination, rather than the objects, which is often violated in specular reflections.

This paper describes several directions that we pursue to counter common deviations from the underlying assumptions of polarization-based dehazing. The method is now more automatic, and presents better results. In addition, we describe an initial study into the use a liquid crystal device in the imaging system, aiming at faster acquisition for dehazing.

2. THEORETICAL BACKGROUND

In this section we describe the principles behind the basic dehazing algorithm of Ref. 13. Consider Fig. 1. When acquiring an outdoor scene, the resulting image is a combination of two main components. The first originated from the object

Further author information: (Send correspondence to E.N.)

E.N.: E-mail: einav@ee.technion.ac.il

Y.Y.S.: E-mail: yoav@ee.technion.ac.il

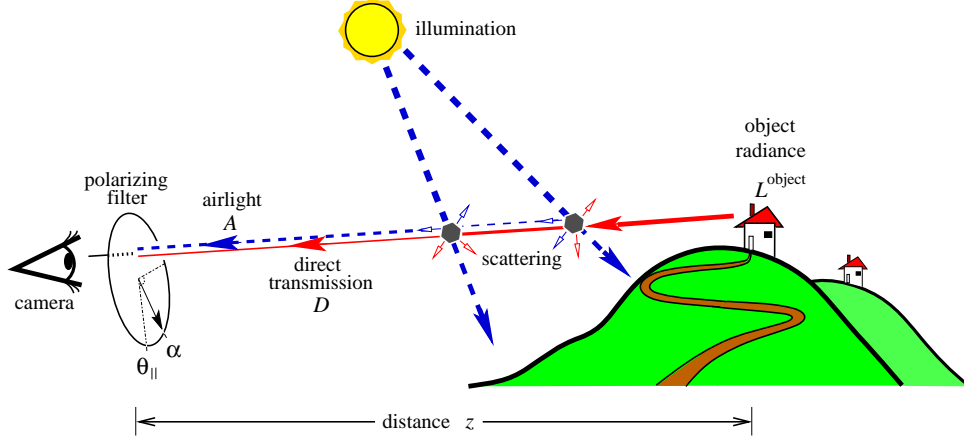


Figure 1. (Dashed rays) Light coming from the sun and scattered towards the camera by atmospheric particles is the airlight A . (Solid ray) Light emanating from the object L^{object} is attenuated by the medium along the line of sight, resulting in direct transmission D . Both A and D depend on the distance z . The scene is imaged through a polarizing filter oriented at angle α .

radiance. Let us denote by L^{object} the object radiance as if was taken in a clear atmosphere, without scattering on the line of sight. Due to attenuation in the atmosphere, the camera senses a fraction of this radiance,^{*} which is the direct transmission

$$D = L^{\text{object}}t, \quad (1)$$

where

$$t = e^{-\beta z} \quad (2)$$

is the transmittance of the atmosphere. The transmittance depends on the distance z between the object and the camera, and on the atmospheric attenuation coefficient β .

The second component is known as *path radiance*, or *airlight*. It originates from the scene illumination (e.g., by the sun), portion of which is scattered into the line of sight by atmospheric particles. It is given by

$$A = A_{\infty}(1 - t), \quad (3)$$

where A_{∞} is the of airlight, which depends on the atmospheric and illumination conditions. Contrary to the direct transmission, this component increases with the distance and dominates the acquired image irradiance

$$I_{\text{total}} = D + A \quad (4)$$

at long range. This is a major cause for reduction of image contrast in haze.

In haze, the airlight is often partially polarized. Hence, we can modulate it by mounting a polarizing filter at angle α in the imaging system. When rotating the polarizer, there is an orientation at which the image is least intense. Let us denote this image as I_{min} . Ref. 13 assumes that polarization is associated only with the airlight. If so, then I_{min} corresponds to the lowest amount of airlight. Hence, this is the image with the best contrast that can be achieved by optical filtering. We denote this optimal polarizer orientation as θ_{\parallel} . We may then rotate the polarizer by 90° relative θ_{\parallel} . This time the image irradiance is strongest, since we sense the principle polarization component of the airlight. Denote this image as I_{max} .

Once these images are acquired, Ref. 13 describes dehazing of the scene as estimating

$$\hat{L}^{\text{object}} = \frac{I_{\text{total}} - \hat{A}}{\hat{t}}, \quad (5)$$

^{*}There is a proportion factor between the scene radiance and image irradiance that depends on the imaging system, but does not depend on the medium and its characteristics. We thus leave this factor out.

where

$$\hat{t} = 1 - \frac{\hat{A}}{A_\infty} \quad (6)$$

is the estimated transmittance and

$$\hat{A} = \frac{I_{\max} - I_{\min}}{p} \quad (7)$$

is the estimated airlight. Here p is the degree of polarization of airlight. It is measured from the raw images by looking at pixels which correspond to objects at infinity. We assign such pixels to the sky near the horizon

$$p = \frac{I_{\max} - I_{\min}}{I_{\max} + I_{\min}} \Big|_{z=\infty} . \quad (8)$$

Similarly, the airlight saturation value is estimated from the same sky area as

$$A_\infty = [I_{\max} + I_{\min}]_{z=\infty} . \quad (9)$$

Based on Eqs.(2,6), a scaled distance map of the scene is recovered

$$\beta \hat{z} = -\log \left[1 - \frac{\hat{A}}{A_\infty} \right] . \quad (10)$$

This operation is done in each color channel separately.

3. IMPROVED DEHAZING ALGORITHM

Sec. 2 briefly describes the method detailed in Ref. 13. That method has been formulated rather naively. There are scenarios in which the underlying assumptions do not hold. Moreover, it has not accounted for the limited dynamic range of display devices. In addition, it had somewhat inconvenient features, as the need to manually detect a sky region for measuring A_∞ and p , and the practice of mechanically rotating a polarizing filter in the imaging system. In this section we address faults in the algorithmic aspects. Sec. 4 discusses efforts to improve the hardware.

3.1. Handling Specular Objects

The method described in Ref. 14 assumes that polarization is associated only with the airlight. However, specular dielectric objects, such as water bodies (lakes) and shiny construction materials (e.g., windows) reflect light towards the camera that can be significantly polarized.^{9, 15, 16, 20} If such objects are close, then the electric field associated with their polarization may dominate over the partially polarized airlight.

The method in Ref. 14 would thus misinterpret such measurements. Typically, the result then is of highly exaggerated airlight and distance estimation at pixels corresponding to close-by specular objects. Subsequently, such pixels are over-compensated, often to strange colors or darkness. As an example, in Fig. 2 we can see specular objects (a water reservoir and nylon sheets) in the hazy image.[†] The basic method¹⁴ of dehazing (middle) produces black spots in these areas, in conjunction to anomalous distance estimation (right). We note that all of the raw images in this paper were acquired using a Nikon D100 camera, which has a linear radiometric response.⁶

Correction is done by image analysis tools. We exploit the fact that often such problematic image areas are isolated. While most of the image is well behaved, it includes rather small anomalous areas. These areas are easily spotted in the airlight image. This image is equivalent to the distance map, and is typically very smooth: adjacent objects may have different albedo, but if their distance from the camera is similar, then their airlight value should be similar. Hence, our algorithm automatically detects areas in the airlight image that are very different from their surroundings. In those areas, the naively estimated airlight is considered unreliable. There, the airlight is automatically re-estimated by simple interpolation of the airlight values of the surroundings.

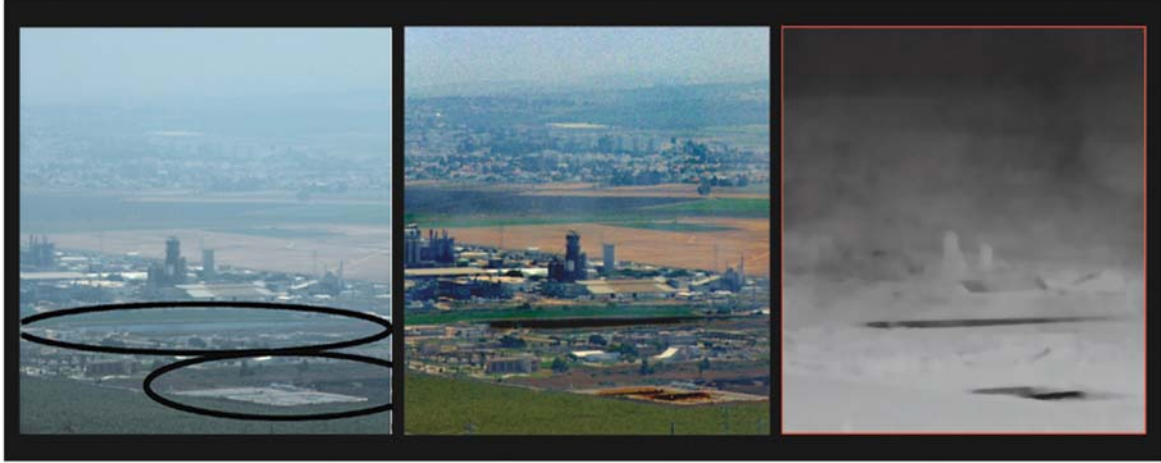


Figure 2. Naive dehazing when specular objects exist in the field of view. [Left] The best-polarized image of the scene, I_{\min} . Note the specular objects (water reservoir, nylon sheets).[Middle] In the naively dehazed image, the color has distorted to black in the specular objects area. [Right] The range map shows anomalies in those areas as well. **For high resolution color images, link to Ref. 11**

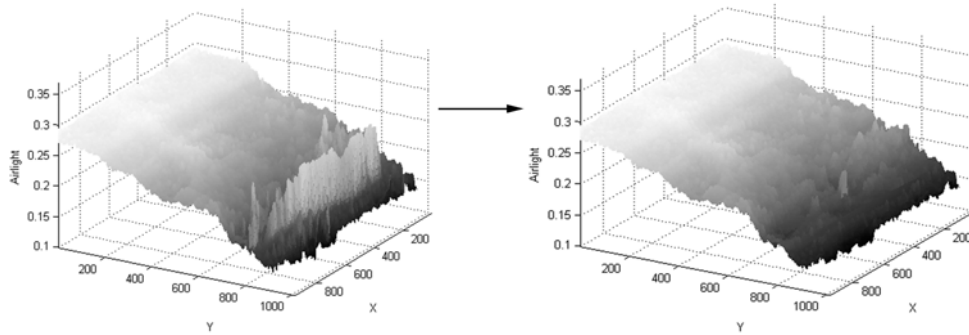


Figure 3. The airlight map. [Left] Uncorrected. [Right] Corrected.

Fig. 3 plots a mesh representation of the airlight $A(x, y)$ estimated from the scene mentioned in Fig. 2. The problematic areas change abruptly relative to their close surroundings. These areas have been automatically detected and corrected by our algorithm to gradually change, based these surroundings.

The corrected airlight is then used to obtain a better transmittance (distance) map. The raw images are then compensated for the effects of haze using Eq. 5, where the corrected airlight and transmittance maps are inserted as t and A . This eliminates the above mentioned problems. Relating to the example above, Fig. 4 shows the improved results. We now regularly apply this automatic method in our experiments.

3.2. Color Correction by Dynamic Range Compression

In this section we describe a problem caused by incompatibility of the naive algorithm with the limited dynamic range of display hardware. The problem leads to distortion of colors and contrast in \hat{L}^{object} . We then use a standard image processing tool to counter this problem.

[†]For clarity of display, the brightness of the displayed pictures in this paper underwent the same standard contrast enhancement (stretching), while their hue and color saturation were untouched. The recovery algorithms, of course, have used the raw (not brightness enhanced) images.



Figure 4. Corrected dehazing when specular objects exist in the field of view. [Left] The best-polarized image of the scene, I_{\min} . [Middle] Result of dehazing accounting for anomalous areas. The colors are recovered, in contrast to the situation in Fig. 2. [Right] The range map is much better behaved than the one in Fig. 2. **For high resolution color images, link to Ref. 11**

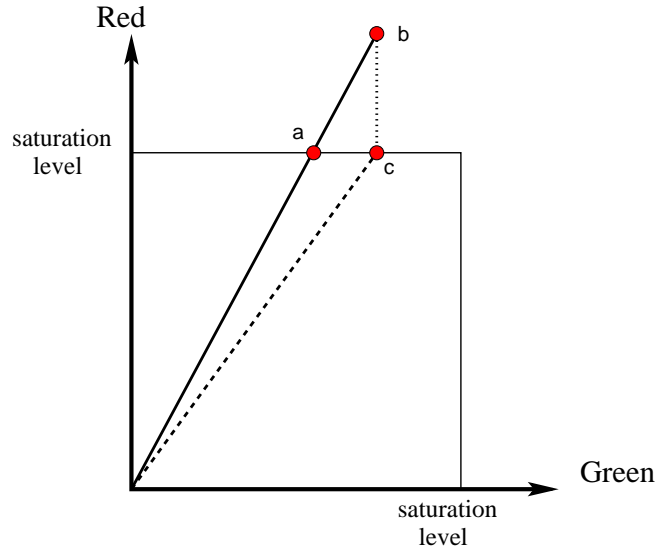


Figure 5. Color distortion by dynamic range overflow. Shown here the Red-Green color subspace. Suppose the dehazed color at a pixel is vector b . Its red component cannot be displayed. If this component is clipped to the red saturation value c , then color is distorted, since the balance between the color components is not conserved. Changing the pixel color to a does not distort the chroma, but luminance information is lost. This loss results in the inability to distinguish nearby pixels having the same chroma, but different luminance values.

As described in Sec. 2, the dehazed image \hat{L}^{object} uses amplification to compensate for atmospheric attenuation. However, in some pixels the amplification may lead to pixel values that are too bright to be displayed. This occurs especially in distant pixels, for which the compensating amplification is very high, and the SNR is low. This problem is compounded by errors in the transmittance, equivalent to errors in the estimated range map z .

This problem is illustrated in Fig. 5. From this figure, it is clear that color clipping results in color distortion. On the other hand, pointwise decrease of luminance leads to indistinguishability of adjacent pixels on the basis of luminance. As an example, Fig. 6(a) shows a hazy scene, as acquired using the best state of the polarizer θ_{\parallel} . Fig. 6(b) shows a result obtained by naive dehazing. While the contrast improved, there are color distortions due to excessive pixel values in \hat{L}^{object} , especially in distant objects by the horizon.

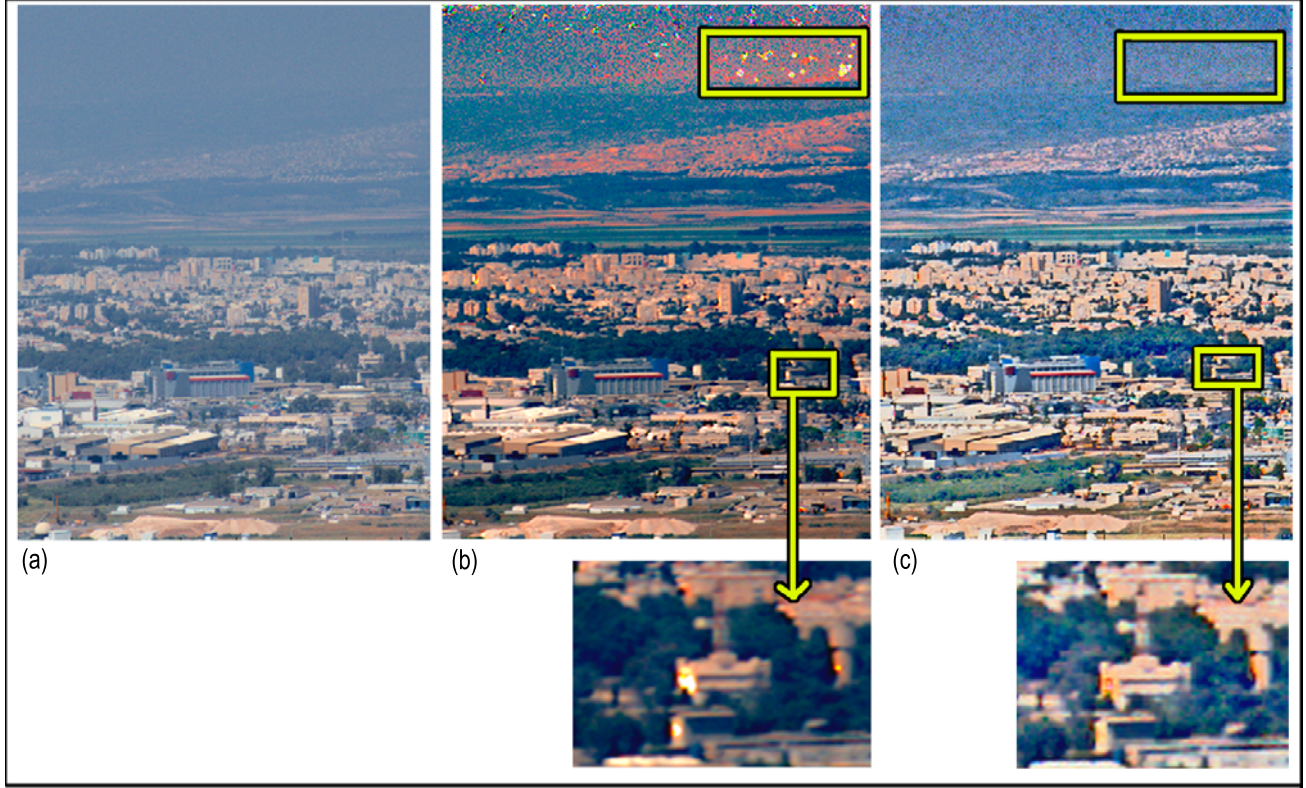


Figure 6. (a) The best polarized raw image, I_{\min} . (b) When displaying the result of naive dehazing, some areas have color distortions caused by overflow of the dynamic range (note the marked areas). (c) Using dynamic range compression of the dehazed image helps to reduce this problem. **For high resolution color images, link to Ref. 11**

This problem is alleviated by applying *dynamic range compression*, which is a general well known method.¹ This method basically enhances details by the following steps:

1. Transferring the color space of the dehazed image $\widehat{L}^{\text{object}}$ from RGB to HSV space, where H,S and V denote hue, saturation and luminance, respectively.

$$\begin{bmatrix} L_H \\ L_S \\ L_V \end{bmatrix} = f \begin{bmatrix} \widehat{L}_R^{\text{object}} \\ \widehat{L}_G^{\text{object}} \\ \widehat{L}_B^{\text{object}} \end{bmatrix}. \quad (11)$$

Here f is the function for transforming the color space, as described in Ref. 5.

2. Dividing the luminance image $\widehat{L}_V^{\text{object}}$ by different factors to create artificial images, to emulate different exposures of the same scene.

$$L_V^{(l)} = \frac{L_V}{C^l}, \quad (12)$$

where $l = 1, 2..n$ is an exposure index, n is total number of artificial images (exposures) created, and C is a constant. Then, in any of these images, the dynamic range of the display is imposed by clipping:

$$V^{(l)}(x, y) = \begin{cases} L_V^{(l)}(x, y) & \text{if } L_V^{(l)}(x, y) < 1 \\ 1 & \text{otherwise} \end{cases}. \quad (13)$$

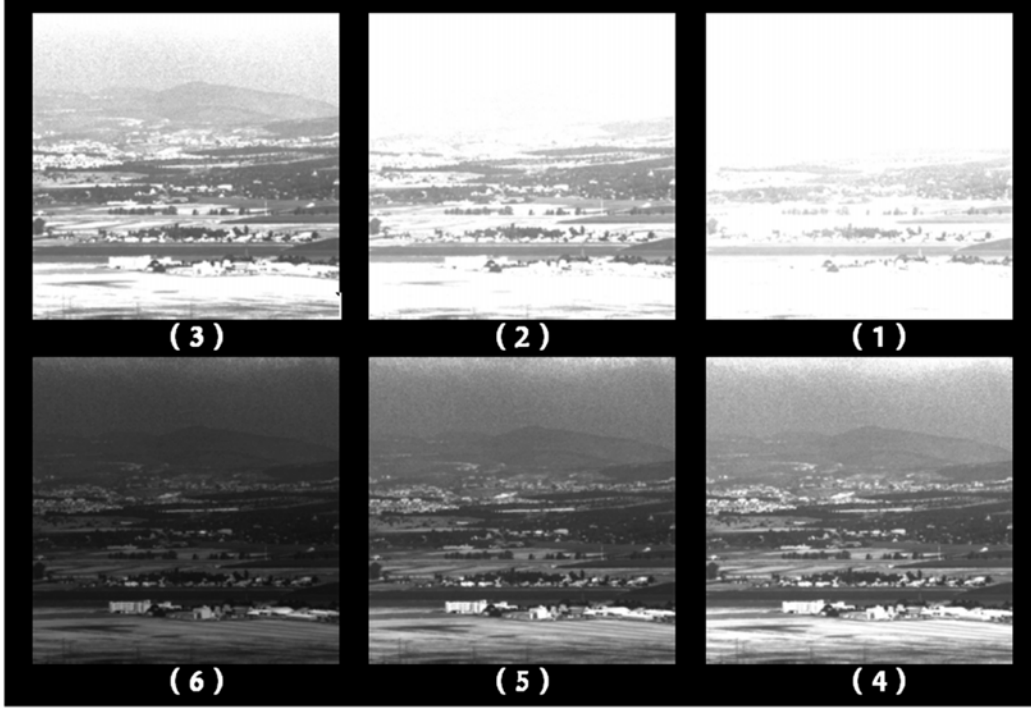


Figure 7. The luminance channel is divided by different values, creating artificial images as if acquired in different exposures.

The constant n in Eq. (12) is thus constrained by

$$C^n > \max(\widehat{L}_V) . \quad (14)$$

This ensures that for every pixel (x, y) , at least one artificial exposure l exists such that $V^{(l)}(x, y)$ is not clipped, hence its information is preserved. Examples of artificial images that are based on an estimated image $\widehat{L}^{\text{object}}$ can be seen in Fig. 7.

3. Creating a Gaussian pyramid^{1,2} for each image $V^{(l)}$.
4. Creating a new image \widehat{L}'_V , which contains all the spatial details that exist in the set $\{V^{(l)}\}_{l=1}^n$. This is done by performing standard image fusion² to this set, for example, using the Gaussian pyramid of each exposure^{1,2}:

$$L'_V = g \left[\left\{ \left\{ V_V^{(l)} \right\}_{l=1}^n \right\} \right] , \quad (15)$$

where g denoted the fusion operator.²

5. Using L'_V as a luminance image, and merging it with the original chromatic channels L_H and L_S .
6. Transferring back the color space from HSV to RGB:

$$\begin{bmatrix} \widetilde{L}_R^{\text{object}} \\ \widetilde{L}_G^{\text{object}} \\ \widetilde{L}_B^{\text{object}} \end{bmatrix} = f^{-1} \begin{bmatrix} L_H \\ L_S \\ L'_V \end{bmatrix} . \quad (16)$$

Fig. 6(c) shows the result of dehazing with consecutive dynamic range compression. The colors are better displayed.

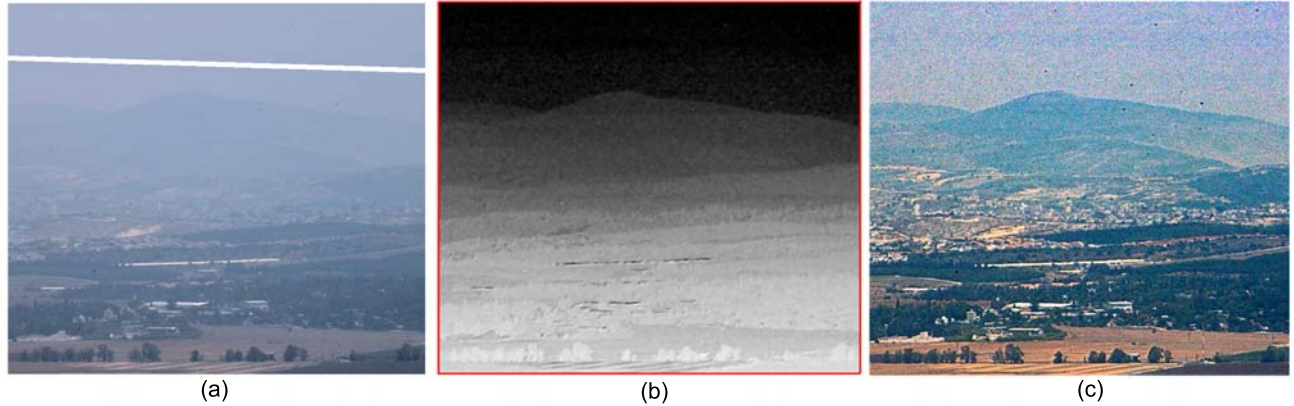


Figure 8. (a) The best polarized image I_{\min} of a hazy scene. The detected *sky* is marked by a line. (b) The estimated distance map. (c) Result of dehazing, including all the algorithmic steps mentioned in this paper, and relying on the automatically selected sky line.

3.3. Automatic Sky Detection

The method has two essential parameters, the airlight properties A_{∞} and p . According to Ref. 14, these parameters can be extracted from the raw images, in areas that correspond to objects at infinity. An appropriate image area is the sky close to the horizon. In Ref. 14, such pixels were manually selected.

We wish to automate this process. Care should be taken. Apparently, the best chance of detecting the sky is to look at the top of the field of view. However, highly oblique lines of sight pass through atmospheric layers having varying aerosol densities. Hence, such measurements do not properly represent the airlight parameters close to the ground. On the other hand, if lower areas in the frame are considered, this may lead to a false interpretation of distant and very hazy objects as the sky, leading to erroneous values.

We thus developed an automatic *sky detector*. It associates the horizon sky with a line across the field of view. This line optimizes a cost function that is based on several image features. These include color, homogeneity, elevation in the field of view, and the lateral slope the line. An example is shown in Fig. 8, where the detected line is marked in white. We note that we apply this method automatically and routinely in our experiments, including those shown in Figs. 2,4, and 6.

4. FAST ACQUISITION BY A LIQUID CRYSTAL MODULATOR

So far, we have performed experiments by mechanically rotating a polarizing filter mounted on the camera. Such an operation is slow. To enable dehazing in video, there is need to switch quickly the state of the polarizer. For this purpose, we now test the feasibility of using a liquid crystal (LC) optical modulator to perform the switching. While we still do not demonstrate dehazing in video, we currently assess the LC technology using still photography.

We use a LC device by Equinox Corp. (New York, NY). This device has a large area, $\approx 7 \times 7\text{cm}$, which enables its easy deployment in front of most camera lenses. It can switch at frame rate speed. It has four states, corresponding approximately to a 45° pitch between orientations of a polarization analyzer. The states are switched via computer commands. A polarizing sheet is attached to the LC cells.

LC-based devices are not a perfect analyzers. The one we worked with performs best in a green band, with apparently poor performance in the blue. This may be satisfactory in most applications, since natural light, as well as human sensitivity peak in the green range. We thus show in Fig. 9 a monochrome experiment based on the green channel of the camera. While the method did improve visibility, the gain appears marginal in this case. We should note that mechanically rotating a simple polarizer in front of the camera yielded raw images that eventually resulted in a much more dramatic improvement. This situation occurred in various other experiments as well.

Unfortunately, the blue component dominates airlight in haze. We hypothesize that for dehazing, an LC should have a wider band of effective performance, with emphasis on the blue portion of the spectrum. It may well be that high quality results would be obtained by tuning the manufacture of LC devices to the spectral needs of this application.

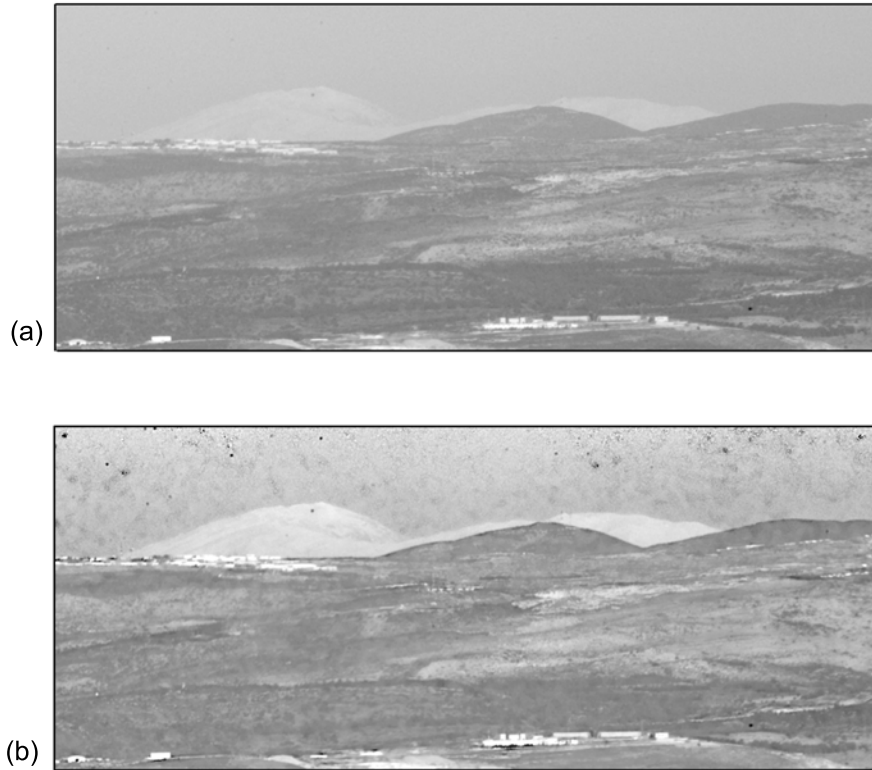


Figure 9. (a) The best polarized green-channel image (I_{\min}) of a hazy scene, acquired via a liquid crystal polarization modulator. (b) The dehazed image. In this experiment the method exhibits a minor improvement.

5. DISCUSSION

Polarization based dehazing is rather new. Due to this reason, it has so far been expressed in a very simple and basic form. Such a form is not reliable for massive use. This work is thus part of a process of making the method more reliable and useful. It addresses some of the problems encountered in the basic formulation, as anomalies caused by specularities, color distortions caused by compensation that is too strong for the display dynamic range, and detection of sky. Additional work certainly needs to be done to further reach the goal of making the method fool proof. In addition, further research and development of hardware is needed to obtain fast acquisition that does not compromise the dehazing performance.

It is worth considering applying such corrections in other domains. Motivated by polarization sensitivity in marine animals,^{3, 17-20} it has recently been shown that underwater path radiance can be compensated for¹² by analysis of polarization-filtered images. Therefore, some of the problems addressed in the current paper with regard to haze may apply underwater, or in other media.

ACKNOWLEDGMENTS

Yoav Schechner is a Landau Fellow - supported by the Taub Foundation, and an Alon Fellow. The research was supported by the Israel Science Foundation (grant no. 315/04), and the Magnetron program of the Israeli Ministry of Commerce. The work was done in collaboration with EIOp Ltd. and conducted in the Ollendorff Minerva Center in the Elect. Eng. Dept. at the Technion. Minerva is funded through the BMBF.

REFERENCES

1. E. H. Adelson, C. H. Anderson, J. R. Bergen, P. J. Burt and J. M. Ogden, "Pyramid methods in image processing," *RCA Engineer* 29-6, pp. 33-41 (1984).

2. P. J. Burt and R. J. Kolczynski, "Enhanced image capture through fusion," *Proc. IEEE Int. Conf. Comp. Vis.*, pp. 173-182 (1993).
3. T. W. Cronin, N. Shashar, R. L. Caldwell, J. Marshall, A. G. Cheroske, and T. H. Chiou, "Polarization vision and its role in biological signaling," *Integrative and Comparative Biology*, vol. 43, pp. 549-558 (2003).
4. L. J. Denes, M. Gottlieb, B. Kaminsky, and P. Metes, "AOTF polarization difference imaging," *Proc. SPIE Advances in Computer-Assisted Recognition*, vol. 3584, pp. 106-115 (1999).
5. A. K. Jain, *Fundamentals of digital image processing*, pp. 66-71, Prentice-Hall, Englewood Cliffs, N.J. (1989).
6. N. Karpel and Y. Y. Schechner "Portable polarimetric underwater imaging system with a linear response," *Proc. SPIE 5432: Polarization: Measurement, Analysis and Remote Sensing VI*, pp. 106-115 (2004).
7. N. S. Kopeika, *A system engineering approach to imaging*, pp. 446-452, SPIE Press, Bellingham (1998).
8. J. P. Oakley, "Improving image quality in poor visibility conditions using a physical model for contrast degradation," *IEEE Trans. on Image Processing*, vol. 7, pp. 167-179 (1998).
9. D. Miyazaki, M. Saito, Y. Sato, and K. Ikeuchi, "Determining surface orientations of transparent objects based on polarization degrees in visible and infrared wavelengths," *J. Opt. Soc. Amer. A*, vol. 19, no. 4, pp. 687-694 (2002).
10. S. G. Narasimhan and S. K. Nayar, "Vision and the atmosphere," *Int. J. of Computer Vision*, vol. 48, pp. 233-254 (2002).
11. Y. Y. Schechner, Home page. Follow the link to publications. [http : //www.ee.technion.ac.il/ ~ yoav/](http://www.ee.technion.ac.il/~yoav/)
12. Y. Y. Schechner and N. Karpel, "Clear underwater vision," *Proc. IEEE Computer Society Conf. on Computer Vision and Pattern Recognition*, vol. I, pp. 536-543 (2004).
13. Y.Y. Schechner, S. G. Narasimhan and S. K. Nayar, "Instant dehazing of images using polarization," *Proc. IEEE CVPR*, Vol. I, pp. 325-332, (2001).
14. Y. Y. Schechner, S. G. Narasimhan and S. K. Nayar, "Polarization-based vision through haze," *Applied Optics* 42, pp. 511-525 (2003).
15. Y. Y. Schechner and S. K. Nayar, "Generalized Mosaicing: Polarization Panorama," *IEEE Trans. Pattern Analysis and Machine Intelligence*, Vol. 27, pp. 631-636 (2005).
16. Y. Y. Schechner, J. Shamir, and N. Kiryati, "Polarization and statistical analysis of scenes containing a semi-reflector," *J. Opt. Soc. Amer. A*, vol. 17, pp. 276-284 (2000).
17. N. Shashar, R. Hagan, J. G. Boal, and R. T. Hanlon, "Cuttlefish use polarization sensitivity in predation on silvery fish," *Vision Research*, vol. 40, pp. 71-75 (2000).
18. T. H. Waterman, "Polarization sensitivity," *Handbook of Sensory Physiology*, vol. VII/6B, ch. 3, pp. 281-469. Springer-Verlag, Berlin (1981).
19. R. Wehner, "Polarization vision - a uniform sensory capacity?" *J. Experimental Biology*, vol. 204, pp. 2589-2596, (2001).
20. L. B. Wolff, "Polarization vision: a new sensory approach to image understanding," *Image & Vision Comp.*, vol. 15, pp. 81-93 (1997).